RESEARCH ARTICLE

ENERGY STORAGE WILEY

# New shape-stabilized phase change materials obtained by single-screw extruder

Rebeca Salgado-Pizarro[1] | Guilllermo Ulldemolins[1] | Maria Elena Navarro[2] |
Anabel Palacios[2] | Alejandro Calderón[1] | Yulong Ding[2] |
A. Ines Fernández[1] | Camila Barreneche[1]

[1]Department of Materials Science and Physical Chemistry, Universitat de Barcelona, Barcelona, Spain

[2]Brimingham Center of Energy Storage, School of Chemical Engineering, University of Birmingham, Birmingham, UK

**Correspondence**
Camila Barreneche, Department of Materials Science and Physical Chemistry, Universitat de Barcelona, C/Martí i Franquès 1, 08028 Barcelona, Spain.
Email: c.barreneche@ub.edu

**Funding information**
Agència de Gestió d'Ajuts Universitaris i de Recerca, Grant/Award Number: DIOPMA 2017 SGR 0118; Agència per la Competitivitat de l'Empresa ACCIO10, Grant/Award Number: TECNIO; Ministerio de Economía y Competitividad, Grant/Award Number: RTI2018-093849-B-C32 (MINECO/FEDER)

**Abstract**

Shape-stabilized phase change materials (SS-PCM) are promising materials given their potential to control leakage of liquid PCM. However, SS-PCM still has low thermal conductivity and high flammability, which are important properties for several applications, such as the thermal indoor comfort in buildings. In this study, two new polymeric SS-PCM were developed and their properties were optimized by the use of different additives. Both high-density polyethylene (HDPE) and polyoxymethylene (POM) work as matrix materials and MPCM 28 from Microtek acts as PCM. Besides, the graphite was used as an additive material to increase the thermal conductivity, and the magnesium hydroxide to minimize flammability of the composite. Both inorganic fillers also help in the PCM dispersion within the matrix. To evaluate the effect of each component, seven formulations were manufactured by a single screw extruder and a set of characterization (Differential scanning calorimetry, Thermogravimetric analyses, for thermophysical evaluation, and dynamical mechanical analyses, for thermomechanical evaluation over 1000 thermal cycles was performed. The main outputs of the investigation are the proposed formulations that have a good fire reaction performance, whereas their thermal and chemical stability are guaranteed up to 1000 cycles. The HDPE samples present around 12 kJ/kg melting enthalpy when 10 wt% microencapsulated PCM is included in the formulation. In addition, the POM samples present around 7.5 kJ/kg when 10 wt% microencapsulated PCM is included in the formulation. For all formulations, the melting enthalpy obtained is around 27.5°C, in concordance with the reported by the manufacturer.

**KEYWORDS**
cascade PCM, extrusion, phase change materials, polymer-based PCM, shape-stabilized PCM

# 1 | INTRODUCTION

One of the greatest challenges to be addressed in our modern society is the current high energy consumption rates. In such energy scenario, one of the most energy-demanding sectors is commercial and private buildings.[1,2] The building sector is responsible for 36% of global final energy consumption, which is approximately 40% of the total overall direct and indirect $CO_2$ emissions. Besides, the units used to conditionate buildings indoors, for services such as heating, ventilating and air conditioning, account for the 50% of the total energy consumed by that sector.[3] The main concern in the sector is that non-renewable energies are the main sources used to satisfy its energy demand. For that reason, thermal energy storage (TES) systems in buildings have gained attention in recent years as can potentially reduce the energy consumption from cooling and heating systems. The estimated energy reduction is driven by (1) switching the peak demand, (2) reducing the maximum peak of consumption and (3) filling the gap between the energy supplied and the energy demand.[4]

Current TES technologies are mainly based on sensible heat, this kind of store is well-known to be limited by a low energy density, low performance of storage materials and excessive thermal losses.[5,6] Latent heat TES (LHTES) uses the heat involved in a phase change material (PCM) transition. LHTES has shown great potential to be implemented in building envelopes, reducing up to 25% of the energy consumption in buildings.[7,8] The incorporation of the PCMs in buildings has been studied for several applications; in wallboard[9] that provides thermal storage distributed throughout the building indoors; in concrete walls by incorporating microencapsulated PCMs (mPCMs),[10,11] which is a way to produce low-cost storage materials with structural and thermostatic properties, in building insulation materials[12]; or as part of one layer of the envelope as shape-stabilized PCMs (SS-PCMs).[13]

LHTES have high storage densities across a wide temperature range ($-30°C$-$1000°C$), and the most common transition is the solid-liquid one.[14–16] Generally, organic PCM presents low thermal conductivity, which limits the charge and discharge processes speed. For this reason, a high heat transfer surface is required to guarantee the optimal behaviour of the PCM.[17] Besides, PCMs present leakage problems, cost intensive raw materials and large-scale manufacturing limitations; this is translated on low technology readiness level (TRL).[18,19] In this scenario, the use of SS-PCM, which consists of a PCMs incorporated in a polymeric matrix, is the most cost-efficient solution to overcome these limitations.[20] Besides, SS-PCM have the potential to incorporate property enhancer additives, such as thermal conductivity enhancer and other components, to improve mechanical strength and flammability.[19,21] Given the flexibility and multicomponent nature of SS-PCM, they bring up the possibility to create a multiple heat storage system, where two or more stores of the SS-PCM operate in different temperature ranges,[23–26] the so-called cascade systems.[22]

Nevertheless, one of the main barriers associated with the scalability of SS-PCMs are the challenges related to the manufacturing as most of the SS-PCM have been fabricated in a laboratory scale, where specific techniques that are unsuitable for continuous large volume production or real conditions are applied.[27] Likewise, it is difficult to establish a relation between formulation and fabrication processes due to the lack of large-scale manufacturing studies.

In this study, the main objective is the use of a continuous extrusion process with a single screw extruder to fabricate the SS-PCMs based on high-density polyethylene (HDPE) and polyoxymethylene (POM) with microencapsulated PCM as a latent heat component. To achieve the main goal, two additives were used carbon graphite (G) as a thermal conductivity enhancer and magnesium hydroxide (M) as a fire retardant. An exhaustive study of the performance of the different fabricated SS-PCMs is presented, evaluating the thermal and chemical stability as well as the thermodynamics and thermal cycling behaviour.

# 2 | EXPERIMENTAL PROCEDURE

## 2.1 | Materials and composite synthesis

Two types of polymers were used as a matrix: high-density polyethylene (HDPE) and polyoxymethylene (POM). Total XSene 55060 High Density Polyethylene (HDPE) was purchased from Total Petrochemicals (FRA) and supplied in ~2 mm pellets form whereas POM was high-quality recycled polymer. A microencapsulated phase change material MPCM 28 from Microtek (mPCM) was as the selected thermal energy storage materials and two different additives were used to improve the thermal conductivity, graphite (G), and the flame reaction, magnesium hydroxide (M), respectively. Graphite powder was supplied by Inoxia Ltd (UK) (98.6% purity carbon graphite powder). The main attributes of the materials used to fabricate the different composites are summarized in Table 1.

A single screw extruder with a 4.5 mm diameter dye was used to manufacture the composites. The different components were mixed and introduced in the hopper. The temperature along the screw of the extruder was controlled from the inlet to the outlet in seven different heating zones from 100°C to 120°C to achieve well mix

**TABLE 1** Properties of the materials used

| Material | Function | $\Delta H$ (J/g) | $T_m$ (°c) |
|---|---|---|---|
| HDPE | Matrix and TES material | 175 | 137 |
| POM | Matrix and TES material | 49 | 135 |
| Micro-encapsulated paraffin | TES material and plasticizer | 185 | 28 |
| Graphite | Thermal conductivity enhancer | — | — |
| Magnesium hydroxide | Flame retardant | — | — |

composite and avoid the degradation of some of the components of the mixture. Extrusion speed and pressure along the screw were monitored during the process. From the combination of the polymers, flame retardant and graphite seven formulations were designed, their compositions and nomenclature for your reference are listed in Table 2. These compositions were studied based on previous extrusion proofs manufactured at our laboratories.

## 2.2 | Characterization

The thermal stability of the composites fabricated was evaluated by a thermocycling test, up to 1000 thermal cycles. Each cycle consists of a heating stage, from 15°C to 45°C at 5°C·min$^{-1}$, an isothermal step at 45°C for 3 minutes and a cooling stage from 45°C to 15°C at 5°C min$^{-1}$. The thermal properties of the cycled samples were then evaluated using differential scanning calorimetry (DSC), the device used was a DSC 822e Star3+ by Mettler Toledo, measuring the enthalpy and the melting temperature of the PCM composites. The tests were performed from 15°C to 180°C with a heating rate of 1°C min$^{-1}$ in a nitrogen atmosphere with a 50 mL min$^{-1}$ of gas flow.

In addition, Fourier-Transform Infrared spectroscopy (FT-IR), Perkin Elmer (Spectrum Two) instrument, was used to evaluate chemical changes caused by the degradation of the samples after the thermocycling test.

A Thermogravimetric Analyser, from TA Instruments (SDT Q600), was used to study the thermal stability and degradation of the samples. The test was carried out at 50 mL min$^{-1}$ N$_2$ gas flow, from 150°C to 500°C with a heating rate of 10°C·min$^{-1}$.

Furthermore, a dripping test was performed to evaluate the flammability behaviour, described in the UNE 23727[28] standard. This test evaluates the flame and its propagation in a fire scenario-case like. SS-PCM samples were weighed and introduced into a ceramic crucible, which was placed on a metallic grid 3 cm below a heat source of 500 W.

Dynamic mechanical analysis (DMA) was used to evaluate the thermomechanical properties of the samples

**TABLE 2** Composition of the different blends prepared

| Sample | wt% | | | | |
|---|---|---|---|---|---|
| | HDPE | POM | mPCM | M | G |
| HDPE | 100 | — | — | — | — |
| HDPE10mPCM | 90 | — | 10 | — | — |
| HDPE10mPCM20M | 70 | — | 10 | 20 | — |
| HDPE 20mPCM20M | 60 | — | 20 | 20 | — |
| POM | — | 100 | — | — | — |
| POM10mPCM | — | 90 | 10 | — | — |
| POM10mPCM3G | — | 87 | 10 | — | 3 |

under study. The instrument used was a DMA Q800 from TA Instruments. Rectangular samples, $35 \times 15 \times 5$ mm, were cut from the prepared composites and analysed using a dual cantilever clamp. The frequency sweep mode was set and the deformation was strain-controlled (0.1%). A temperature ramp was applied from −145°C to 100°C with a heating rate of 3°C min$^{-1}$, the stress applied was 1 Hz.

## 3 | RESULTS AND DISCUSSION

### 3.1 | HDPE-based composites

Figure 1 shows the thermal stability results of the HDPE composites, where the enthalpy and the melting temperature before and after the thermal cycles were evaluated. It should be noted that HDPE10mPCM has less enthalpy than HDPE10mPCM20M, despite the PCM content is the same (10% wt). This result is related to a filler stabilization behaviour, hence helps in the formation of an SS-PCM. After 1000 thermal cycles, a 33%, 27% and 36% enthalpy decrease is detected in HDPE10mPCM, HDPE10mPCM20M and HDPE20mPCM20M, respectively. The melting temperature remains constant after the cycles and slightly increases by the content of PCM and magnesium hydroxide.

Figure 2 shows the thermal decomposition of the HDPE-based composites.[29] The total weight loss was around 89% and 95% for the samples with and without

magnesium hydroxide, respectively. The first decomposition steps were attributed to the oxidative thermal degradation at temperatures up to 435°C, followed by the decomposition of the oxidation products at temperatures up to 500°C.[30] The paraffin containing samples, mPCMs, two additional steps appear, the paraffin decomposition at temperatures up to 370°C and the acrylic shell decomposition at temperatures up to 430°C,[31] which overlaps with the HDPE decomposition. Table 3 presents the
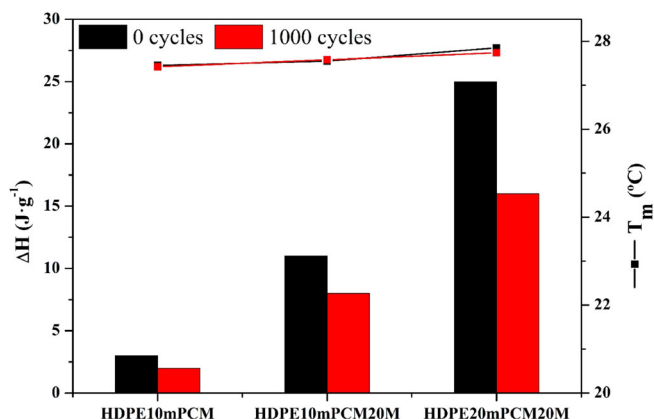


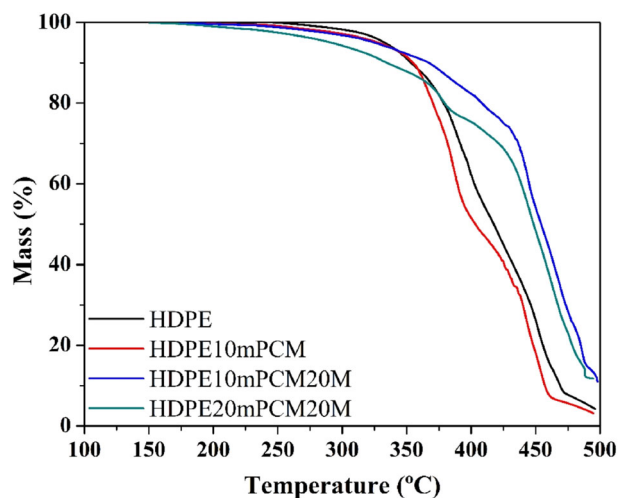**FIGURE 1**  Results of enthalpy and melting temperature at 0 and 1000 cycles



**FIGURE 2**  Thermogravimetric analysis of HDPE-based composites

thermo-oxidative temperatures at 5% and 10% mass loss and the non-volatile inorganic residue at 495°C. The initial thermo-oxidative temperature range at which HDPE10mPCM20M sample loses 5% and 10% of the mass was between 33°C and 34°C, is higher than the HDPE20mPCM20M one.

This might be due to the high content of mPCM in the HDPE20mPCM20M sample that produces a faster thermal degradation leading to lower the thermo-oxidative temperatures than HDEP10mPCM20M sample. Similar behaviour is observed for the samples with and without magnesium hydroxide: the HDPE10mPCM20M sample presents higher values of $T_{10\%}$ than HDPE and HDPE10mPCM samples. This phenomenon can be explained given the fire retardant behaviour of magnesium hydroxide (endothermic decomposition), along with the water release and the formation of a stable oxide around 330°C.[32] Hence, the char residue of these samples is higher than the others.

Figure 3 and Table 4 present the ignition/extinction periods obtained in the dripping test for the different HDPE-based composites. The peaks and the valleys represent the time when the sample ignites and extinguishes respectively, and the average time between the ignition and the extinction represents the combustion time. In the case of the HDPE (see Figure 3A), the dripping test shows that once it is ignited, the HDPE keeps burning until the fuel is exhausted (combustion behaviour). The addition of mPCM (see Figure 3B) curve does not introduce significant changes in the fire behaviour. In contrast, Figures 3C and 4D profiles show a high number of ignition and extinctions during the test; this is related to the fire-retardant behaviour of the magnesium hydroxide. The higher the content magnesium hydroxide, the better self-extinguished flame reaction behaviour measured.

The FT-IR spectra of the different samples, after and before the thermal cycling, are shown in Figure 4, where the three characteristic zones of the mixtures are plotted: 3100-2600 cm$^{-1}$ (A), 1800-1250 cm$^{-1}$ (B) and 1190-450 cm$^{-1}$ (C). Figure 4A shows the 2915 and 2847 cm$^{-1}$ bands of C—H stretching vibrations of the HDPE and paraffin.[33-35] This band is associated with a C—H stretching normally found in polypropylene.[36] Figure 4B presents the 1470 and 1446 cm$^{-1}$ bands of -CH$_2$ bending of the HDPE and the

| | $T_{1\%}$ (°C) | $T_{5\%}$ (°C) | $T_{10\%}$ (°C) | Residue at 495°C (%) |
|---|---|---|---|---|
| HDPE | 282 | 332 | 353 | 4.61 |
| HDPE10mPCM | 255 | 328 | 355 | 3.28 |
| HDPE10mPCM20M | 244 | 325 | 367 | 13.57 |
| HDPE20mPCM20M | 201 | 291 | 334 | 11.78 |

**TABLE 3**  Thermo-oxidative temperatures, at 1%, 5% and 10% of mass loss from initial mass and chart residue

overlapped band of 1466 cm$^{-1}$ of the C—H scissoring of the paraffin.[33–35] In addition, O—H vibration is detected at 1420 cm$^{-1}$ due to the presence of magnesium hydroxide. Figure 4C presents the 730-700 cm$^{-1}$ bands of —CH$_2$ rocking of the HDPE, the overlapped band 720 cm$^{-1}$ of the bending C—H of the paraffin,[33–35] the 876 and 592 cm$^{-1}$ bands are associated to Mg—O—Mg stretching vibration[37] and 482 cm$^{-1}$ bands of Mg—O vibrations.[38] Based on the main FT-IR results obtained, there is

not any degradation process active after the thermal cycling test.

The dynamic mechanical properties of HDPE-based composites as a function of temperature are shown in Figure 5. All the samples present curves corresponding to a semi-crystalline structure, HDPE 80% crystallinity.[39]

The storage modulus ($E'$), plotted in Figure 5A, is proportional to the stiffness of the materials,[40] hence the pure HDPE and HDPE10mPCM20M are the samples which present the highest stiffness. The HDPE 10mPCM and HDPE20mPCM20M present the lowest $E'$ values. The addition of PCM is expected to reduce the storage modulus, while the use of ceramic fillers like magnesium hydroxide, which are stiffer, increase the $E'$. The results show the contribution of these opposite effects, being the mPCM content the most relevant. Figure 5B,C presents the loss modulus ($E''$) and tan($\delta$) curve respectively, in where three main transitions are detected $\gamma$-, $\beta$- and $\alpha$-transitions. The values of peak temperature associated with each transition are summarized in Table 5, extracted from Figure 5B. The $\gamma$- and $\beta$-transitions are associated with chain motion in the amorphous phase and the $\alpha$-transition is directly related to crystalline degree, hence is the lamellar motion in the crystalline phase.[41–45] The $\gamma$-transition of pure HDPE was detected at $-117.63°C$, which is the glass transition temperature ($T_g$).[43,45] The $\alpha$-transition appears at 54.98°C for the pure HDPE, the intensity and $\alpha$-transition temperature ($T\alpha$) decrease and
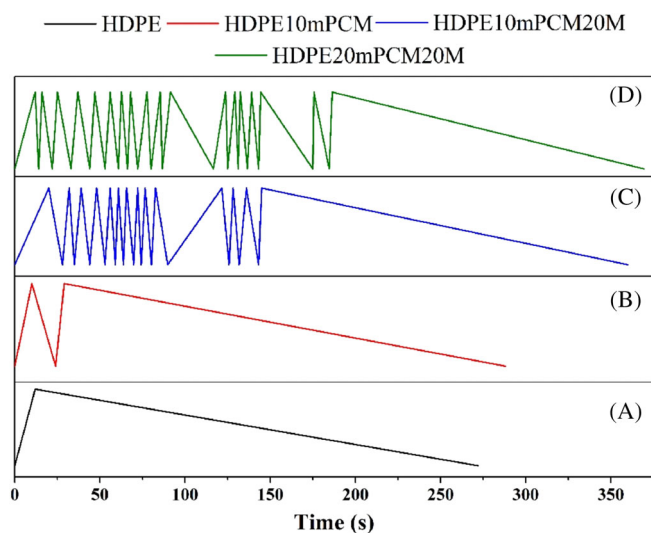


**FIGURE 3** Dripping test results of HDPE-based composites

**TABLE 4** Dripping test results for HDPE-based composite

| Sample | Ignition time (s) | N° of ignitions | Average combustion time (s) |
|---|---|---|---|
| HDPE | 12 | 1 | 272 |
| HDPE10mPCM | 10 | 3 | 288 |
| HDPE10mPCM20M | 20 | 27 | 360 |
| HDPE20mPCM20M | 12 | 37 | 369 |



**FIGURE 4** FT-IR spectra of HDPE-based composites before and after the thermal cycles
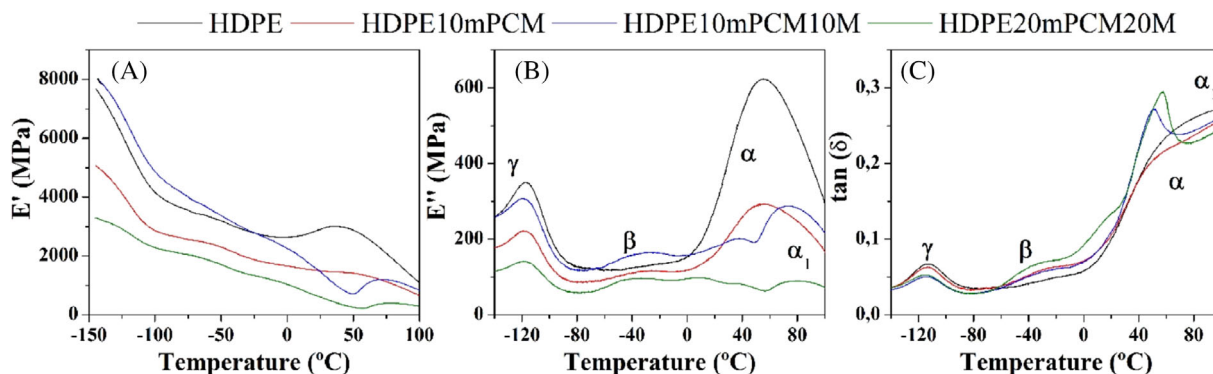
**FIGURE 5** DMA results of HDPE-based composite: A. Storage modulus curve; B. Loss modulus curve; C. Tan(δ) curve

**TABLE 5** Summary of the peak temperature transitions of the HDPE-based composite, extracted from the Loss modulus curve

| Formulation | $T_\gamma$ | $T_\alpha$ | $T_\beta$ | $T_{\alpha1}$ |
|---|---|---|---|---|
| HDPE | −117.63 | 54.98 | — | — |
| HDPE10MPCM | −118.72 | 52.67 | −25.82 | — |
| HDPE10MPCM20M | −120.04 | 37.54 | −31.36 | 74.45 |
| HDPE20MPCM20M | −118.61 | 35.98 | −33.50 | 79.21 |



**FIGURE 6** Enthalpy and melting temperature of POM-based composites

moves to lower temperatures by the addition of the different components. This is triggered by the addition of other components into the HDPE structure, which promotes the formation of thinner and separated lamellas, requiring less energy for relaxation of the hard segments.[43] Also, an $\alpha_1$-transition is detected in the magnesium hydroxide of the manufactured samples, due to the behaviour of the filler as a nucleating agent that promotes an induced crystallization of HDPE at the particle surface.[46] The β-transition is the movement either of the branches or the main chain segment in the amorphous phase.[43] Moreover, β-transition appears in PE samples with a higher percentage of amorphous phase,[42] indicating that the formulations with mPCM and magnesium hydroxide have lower crystallinity than pure HDPE.

## 3.2 | POM-based composites

The thermal stability of the POM based composites is presented in Figure 6. The results show that the graphite containing sample has less enthalpy compared to the sample without graphite. This result can be related to an increase of the thermal conductivity of the sample that improves the heat transfer, but also could be attributed to a bad homogeneity of the sample. After the thermal cycling, a slight decrease of enthalpy in the POM10mPCM sample is detected, a decrease of 3.7%, and in the POM10mPCM3G
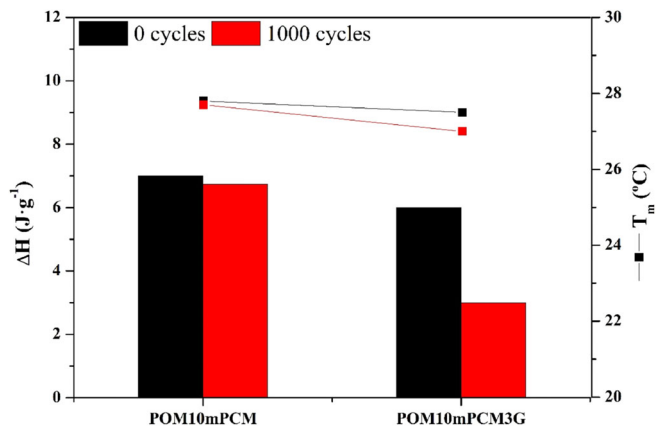
sample, the decrease is even higher, a decrease of 50%. The melting temperature shows values around 27°C in both samples, before and after the thermal cycling.

The thermogravimetric analysis of POM composite samples shows that thermal degradation takes place between 150°C and 500°C. In Figure 7, the mass % and the weight corrected heat flow are plotted. The total weight loss was 97% for the samples without graphite and 88% for the sample with graphite. The decomposition steps attributed to POM were the oxidative thermal degradation at temperatures up to 380°C and the decomposition of the oxidation products at temperatures up to 495°C. The paraffin containing composites show an additional decomposition step in between attributed to the mPCM shell degradation.[31] The thermo-oxidative temperatures at 5% and 10% of mass loss, and the non-volatile matter, the residue at 495°C, are presented in Table 6. The POM and POM10mPCM samples present similar values of $T_{5\%}$ and $T_{10\%}$, which are higher than POM10mPCM3G. In contrast, the sample that presents higher residue is the graphite containing sample. The presence of graphite in the formulation POM10mPCM3G

favours the degradation at a lower temperature, probably because of the higher thermal conductivity improving the heat transfer. Otherwise, the graphite contributes to the stabilization at higher temperatures and clearly induces the formation of a solid char of unburned residue.

Again, the maximum working temperature corresponds to a sample loses of 1% in weight. Therefore, the maximum working temperature is $T_{1\%}$ plotted in Table 6.

The results of the dripping test are illustrated in Figure 8 and Table 7. In the POM sample, Figure 8A, only a single ignition is detected, and the sample keeps burning until the extinction of the fuel (combustion behaviour). By the addition of the mPCM, non-significant changes are observed, the flammability behaviour remains as combustor material. In contrast, with the addition of the graphite, a higher number of ignition and extinction were produced, and a delay on the ignition time is detected, due to the effect of the graphite forming a char with a barrier effect.

Figure 9 shows the FT-IR spectra of the POM based composites, before and after the thermal cycles. The three main regions of the spectra were studied: 3040-2600 cm$^{-1}$ (A), 1780-1160 cm$^{-1}$ (B) and 1200-560 cm$^{-1}$ (C). Figure 9A shows the 2916-2848 cm$^{-1}$ bands corresponding to the C—H stretching of POM and paraffin.[35,47] In this region, no new bands were detected, hence no degradation was

detected. Figure 9B presents the 1473-1462 cm$^{-1}$ bands of CH$_2$ bending of the POM and paraffin[34,35] and the 1434-1383 cm$^{-1}$ bands of —CH$_3$ and the 1237 cm$^{-1}$ band C—O—C bending are associated to the POM.[47,48] Also, a low-intensity extra band around the 1741 cm$^{-1}$ is detected, due to the presence of a carbonyl group, meaning that some oxidation took place during cycling or the shaping process.[48] Figure 9C shows the asymmetric and symmetric bands of skeletal stretching of C—O—C at 1089, 932 and 902 cm$^{-1}$, the CH$_2$ rocking vibration at 730-719 cm$^{-1}$ and the O—C—O bending at 632 cm$^{-1}$.[47]

The thermomechanical results of the POM based composites are shown in Figure 10, where the behaviour of a semi-crystalline polymer is observed.[39] Figure 10A presents the $E'$ curve showing that at low temperature ($T < 0°C$) the POM10mPCM3G has the highest stiffness while above higher temperatures ($T > 0°C$) the three samples present similar stiffness. Figure 10B presents the $E''$ curve and (C) the tan($\delta$) curve, in where two of the three main transitions of POM are observed: $\beta$- and $\gamma$-transitions and the glass transition $\gamma$-transition.[49] The $\beta$-transition is a cooperative motion of long chains in the amorphous phase that is observed after a fast cooling and disappear with ageing at room temperature. The sample POM10mPCM3G clearly shows this peak, due to the presence of graphite increasing the thermal conductivity and thus the heat transfer during cooling. The PCM also affect the cooling, and the peak of this transition is lower in the POM10mPCM sample than the graphite sample, while it is not observed in the pure POM. The $\alpha$-transition is not detected as it happens at 130°C,[49] but
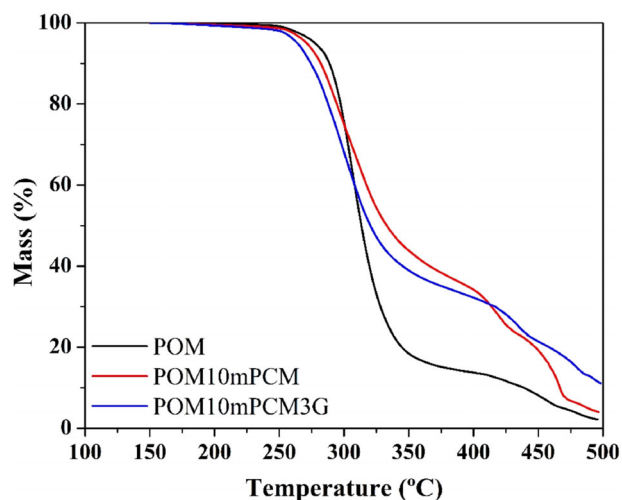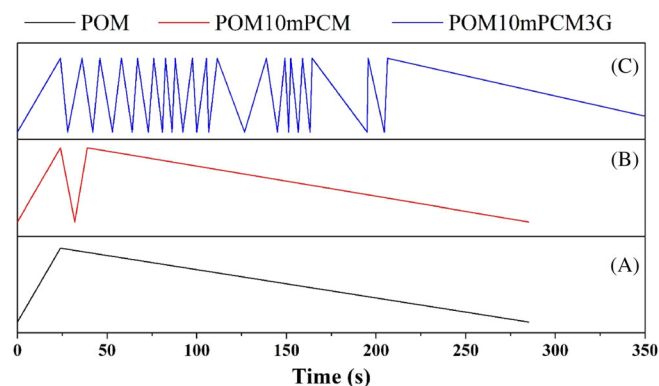


**FIGURE 7**  TGA of POM-based composites



**FIGURE 8**  Dripping test results of POM-based composites

**TABLE 6**  Thermo-oxidative temperatures at 1%, 5% and 10% of mass loss from initial mass and chart residue

|  | $T_{1\%}$ (°C) | $T_{5\%}$ (°C) | $T_{10\%}$ (°C) | Residue at 495°C (%) |
| --- | --- | --- | --- | --- |
| POM | 253 | 277 | 288 | 2.29 |
| POM10mPCM | 238 | 271 | 281 | 4.27 |
| POM10mPCM3G | 218 | 264 | 274 | 11.70 |

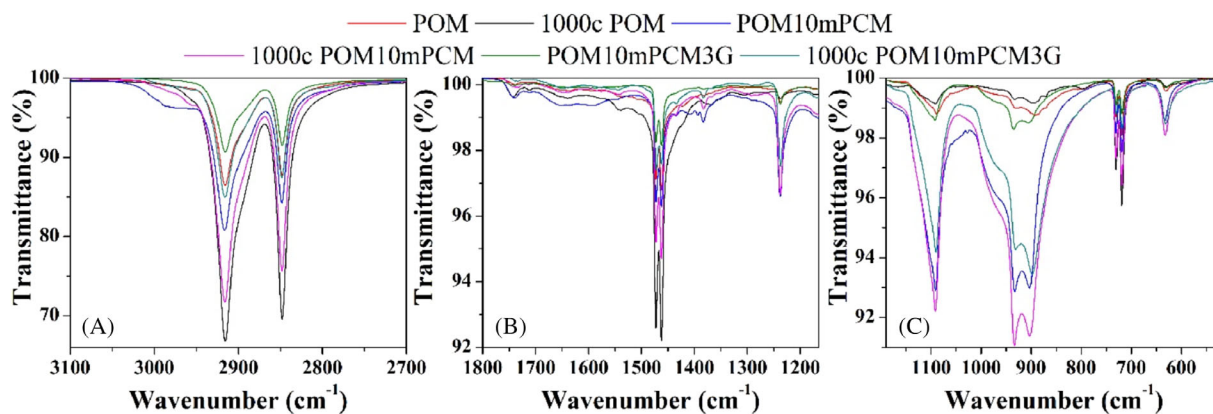| Sample | Ignition time (s) | N° of ignitions | Average combustion time (s) |
|---|---|---|---|
| POM | 24 | 1 | 285 |
| POM10mPCM | 24 | 3 | 285 |
| POM10mPCM3G | 24 | 35 | 389.4 |



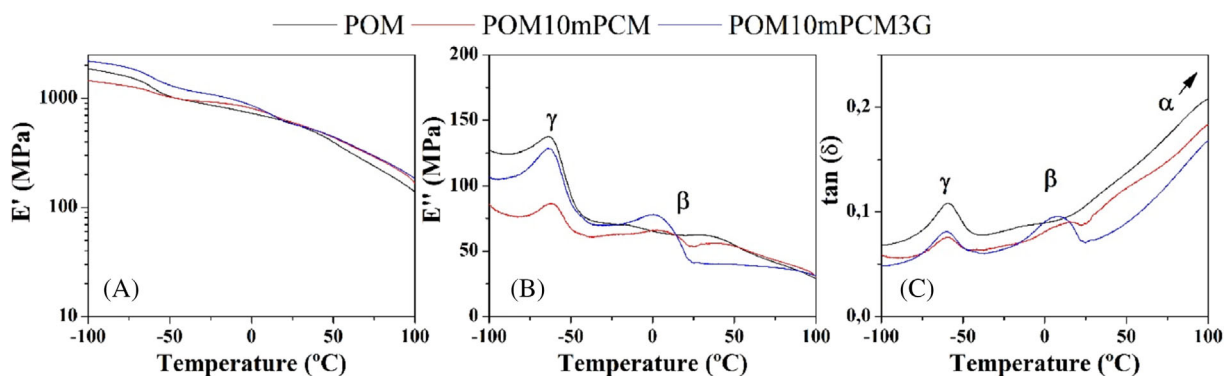**FIGURE 9** FT-IR spectra of POM-based composites



**FIGURE 10** DMA results of POM-based composites

in Figure 10C, it can be seen that $\tan(\delta)$ values for three samples continuously increase with temperature.

## 4 | CONCLUSIONS

In this article, a novel manufacturing route, the single screw extruder, has been applied to obtain the fabrication of a SS-PCM. Seven formulations of polymer-based SS-PCMs were manufactured by using the following components; HDPE and POM as polymeric matrix; microencapsulated PCM; and two additives, graphite and magnesium hydroxide. To ensure the feasibility of the shape-stabilized composites, the samples were cycled for 1000 thermal cycles.

The chemical stability of HDPE composites was demonstrated up to 1000 cycles, due to the FT-IR results, where no changes were detected. Nevertheless, in POM samples indications of degradation were detected. The HDPE and POM based composite are stable over the working temperature range (20°C-200°C) for buildings applications since the maximum working temperature (T1%) for all the samples is higher than 200°C. Besides, the thermal stability is favoured by the flame retardant properties of magnesium oxide, as shown in the dripping test.

The DSC results show an increment of the storage capacity by the addition of magnesium hydroxide, improving the stabilization of the PCM in the matrix. In contrast, the addition of graphite decreases the storage

capacity but an increment in the thermal conductivity is expected. In all the samples, a decrease of enthalpy was detected at 1000 thermal cycles, 33%-36% in HDPE samples, and 4% and 50% in POM samples.

The DMA results show that the mPCM incorporation produces a decrease of the $E'$ especially at lower temperatures for both HDPE and POM composites. Otherwise, the addition of magnesium hydroxide to HDPE composites increases the $E'$ and the results of HDPE composites combine these effects. The graphite addition is less significant for the POM samples. Besides, the incorporation of mPCM in the HDPE produces a decrease of the crystallinity as shown in the $\beta$-transition, and the magnesium hydroxide acts as a nucleating agent as observed in $\tan(\delta)$ curves.

Overall, this study proves that extrusion is a viable manufacturing route that can be potentially used for SSPCM fabrication to ease the commercial path of this TES composite by using a polymeric materials conventional route. Although further studies regarding the effect of the extrusion parameters on the TES attributes should be undertaken, this article paves the way for using extrusion in SS-PCMs.

## ACKNOWLEDGMENTS

## DATA AVAILABILITY STATEMENT
The data will be available by demand thorugh an email contact.

## ORCID
*A. Ines Fernández* https://orcid.org/0000-0001-9212-9714
*Camila Barreneche* https://orcid.org/0000-0003-3636-3180

## REFERENCES

1. Internation Energy Agency (IEA), Global energy & $CO_2$ status report. (2017). https://doi.org/10.4324/9781315252056.
2. International Energy Agency (IEA), World energy outlook 2019. https://webstore.iea.org/world-energy-outlook-2019. Accessed March 19, 2020.
3. Saffari M, De Gracia A, Ushak S, Cabeza LF. Economic impact of integrating PCM as passive system in buildings using Fanger comfort model. *Energ Buildings*. 2016;112:159-172. https://doi.org/10.1016/j.enbuild.2015.12.006
4. Barreneche C, Fernández AI, Niubó M, et al. Development and characterization of new shape-stabilized phase change material (PCM)—polymer including electrical arc furnace dust (EAFD), for acoustic and thermal comfort in buildings. *Energ Buildings*. 2013;61:210-214. https://doi.org/10.1016/j.enbuild.2013.02.026
5. Zhang H, Baeyens J, Cáceres G, Degrève J, Lv Y. Thermal energy storage: recent developments and practical aspects. *Prog Energy Combust Sci*. 2016;53:1-40. https://doi.org/10.1016/j.pecs.2015.10.003
6. Chandel SS, Agarwal T. Review of current state of research on energy storage, toxicity, health hazards and commercialization of phase changing materials. *Renew Sustain Energy Rev*. 2017;67:581-596. https://doi.org/10.1016/j.rser.2016.09.070
7. Delgado MCG, Ramos JS, Domínguez SÁ, Ríos JAT, Cabeza LF. Building thermal storage technology: compensating renewable energy fluctuations, *J Energy Storage*. 2020;27:101147. https://doi.org/10.1016/j.est.2019.101147
8. Song M, Niu F, Mao N, Hu Y, Deng S. Review on building energy performance improvement using phase change materials. *Energ Buildings*. 2018;158:776-793. https://doi.org/10.1016/j.enbuild.2017.10.066
9. Chen C, Guo H, Liu Y, Yue H, Wang C. A new kind of phase change material (PCM) for energy-storing wallboard. *Energ Buildings*. 2008;40:882-890. https://doi.org/10.1016/j.enbuild.2007.07.002
10. Pons O, Aguado A, Fernández AI, Cabeza LF, Chimenos JM. Review of the use of phase change materials (PCMs) in buildings with reinforced concrete structures. *Mater Constr*. 2014;64:e031. https://doi.org/10.3989/mc.2014.05613
11. Pomianowski M, Heiselberg P, Jensen RL, Cheng R, Zhang Y. A new experimental method to determine specific heat capacity of inhomogeneous concrete material with incorporated microencapsulated-PCM. *Cem Concr Res*. 2014;55:22-34. https://doi.org/10.1016/j.cemconres.2013.09.012
12. Baetens R, Jelle BP, Gustavsen A. Phase change materials for building applications: a state-of-the-art review. *Energ Buildings*. 2010;42:1361-1368. https://doi.org/10.1016/j.enbuild.2010.03.026
13. Barreneche C, Navarro L, de Gracia A, Fernández AI, Cabeza LF. In situ thermal and acoustic performance and environmental impact of the introduction of a shape-stabilized PCM layer for building applications. *Renew Energy*. 2016;85:281-286. https://doi.org/10.1016/j.renene.2015.06.054
14. Mastani Joybari M, Haghighat F, Moffat J, Sra P. Heat and cold storage using phase change materials in domestic refrigeration systems: the state-of-the-art review. *Energ Buildings*. 2015;106:111-124. https://doi.org/10.1016/j.enbuild.2015.06.016
15. Li G, Zheng X. Thermal energy storage system integration forms for a sustainable future. *Renew Sustain Energy Rev*. 2016;62:736-757. https://doi.org/10.1016/j.rser.2016.04.076
16. Sciacovelli A, Navarro ME, Jin Y, et al. High density polyethylene (HDPE)—graphite composite manufactured by extrusion: a novel way to fabricate phase change materials for thermal energy storage. *Particuology*. 2018;40:131-140. https://doi.org/10.1016/j.partic.2017.11.011

17. Gasia J, Miró L, Cabeza LF. Materials and system requirements of high temperature thermal energy storage systems: a review. Part 2: thermal conductivity enhancement techniques, renew. *Sustain Energy Rev*. 2016;60:1584-1601. https://doi.org/10.1016/j.rser.2016.03.019

18. Niedermeier K. *Numerical Investigation of a Thermal Storage System Using Sodium as Heat Transfer Fluid*. Karlsrueh: KIT Scientific Publishing; 2019.

19. Putra N, Rawi S, Amin M, Kusrini E, Kosasih EA, Indra Mahlia TM. Preparation of beeswax/multi-walled carbon nanotubes as novel shape-stable nanocomposite phase-change material for thermal energy storage. *J Energy Storage*. 2019;21:32-39. https://doi.org/10.1016/j.est.2018.11.007

20. Ma B, Adhikari S, Chang Y, Ren J, Liu J, You Z. Preparation of composite shape-stabilized phase change materials for highway pavements. *Construct Build Mater*. 2013;42:114-121. https://doi.org/10.1016/j.conbuildmat.2012.12.027

21. Chriaa I, Trigui A, Karkri M, Jedidi I, Abdelmouleh M, Boudaya C. Thermal properties of shape-stabilized phase change materials based on low density polyethylene, hexadecane and SEBS for thermal energy storage. *Appl. Therm. Eng*. 2020;171:115072. https://doi.org/10.1016/j.applthermaleng.2020.115072

22. Tessier MJ, Floros MC, Bouzidi L, Narine SS. Exergy analysis of an adiabatic compressed air energy storage system using a cascade of phase change materials. *Energy*. 2016;106:528-534. https://doi.org/10.1016/j.energy.2016.03.042

23. Shamsi H, Boroushaki M, Geraei H. Performance evaluation and optimization of encapsulated cascade PCM thermal storage. *J Energy Storage*. 2017;11:64-75. https://doi.org/10.1016/j.est.2017.02.003

24. Crespo A, Barreneche C, Ibarra M, Platzer W. Latent thermal energy storage for solar process heat applications at medium-high temperatures—a review. *Sol Energy*. 2019;192:3-34. https://doi.org/10.1016/j.solener.2018.06.101

25. N'Tsoukpoe KE, Osterland T, Opel O, Ruck WKL. Cascade thermochemical storage with internal condensation heat recovery for better energy and exergy efficiencies. *Appl Energy*. 2016;181:562-574. https://doi.org/10.1016/j.apenergy.2016.08.089

26. Teamah HM, Lightstone MF, Cotton JS. Potential of cascaded phase change materials in enhancing the performance of solar domestic hot water systems. *Sol Energy*. 2018;159:519-530. https://doi.org/10.1016/j.solener.2017.11.034

27. Barreneche C, Navarro ME, Niubó M, Cabeza LF, Fernández AI. Use of PCM-polymer composite dense sheet including EAFD in constructive systems. *Energ Buildings*. 2014;68:1-6. https://doi.org/10.1016/j.enbuild.2013.09.004

28. UNE-23727:1990: Ensayos de Reacción al Fuego de los Materiales de Construcción. *Clasificación de los Materiales Utilizados en la Construcción*. Madrid: Asociacion Espanola de Normalizacion; 1990.

29. Miró L, Barreneche C, Ferrer G, Solé A, Martorell I, Cabeza LF. Health hazard, cycling and thermal stability as key parameters when selecting a suitable phase change material (PCM). *Thermochim Acta*. 2016;627–629:39-47. https://doi.org/10.1016/j.tca.2016.01.014

30. Zanetti M, Bracco P, Costa L. Thermal degradation behaviour of PE/clay nanocomposites. *Polym Degrad Stab*. 2004;85:657-665. https://doi.org/10.1016/j.polymdegradstab.2004.03.005

31. Giro-Paloma J, Barreneche C, Martínez M, Šumiga B, Cabeza LF, Fernández AI. Comparison of phase change slurries: physicochemical and thermal properties. *Energy*. 2015;87:223-227. https://doi.org/10.1016/j.energy.2015.04.071

32. Hornsby PR. The application of magnesium hydroxide as a fire retardant and smoke-suppressing additive for polymers. *Fire Mater*. 1994;18:269-276. https://doi.org/10.1002/fam.810180502

33. Jung MR, Horgen FD, Orski SV, et al. Validation of ATR FT-IR to identify polymers of plastic marine debris, including those ingested by marine organisms, *Mar Pollut Bull*. 2018;127:704-716. https://doi.org/10.1016/j.marpolbul.2017.12.061.

34. Fuensanta M, Paiphansiri U, Romero-Sánchez MD, Guillem C, López-Buendía ÁM, Landfester K. Thermal properties of a novel nanoencapsulated phase change material for thermal energy storage. *Thermochim Acta*. 2013;565:95-101. https://doi.org/10.1016/j.tca.2013.04.028

35. Li H, Fang G, Liu X. Synthesis of shape-stabilized paraffin/silicon dioxide composites as phase change material for thermal energy storage. *J Mater Sci*. 2010;45:1672-1676. https://doi.org/10.1007/s10853-009-4146-8

36. Chércoles Asensio R, Moya MSA, De La Roja JM, Gómez M. Analytical characterization of polymers used in conservation and restoration by ATR-FTIR spectroscopy. *Anal Bioanal Chem*. 2009;395:2081-2096. https://doi.org/10.1007/s00216-009-3201-2

37. Vu AT, Jiang S, Ho K, Lee JB, Lee CH. Mesoporous magnesium oxide and its composites: preparation, characterization, and removal of 2-chloroethyl ethyl sulfide. *Chem Eng J*. 2015;269:82-93. https://doi.org/10.1016/j.cej.2015.01.089

38. Qiu L, Xie R, Ding P, Qu B. Preparation and characterization of Mg(OH)2 nanoparticles and flame-retardant property of its nanocomposites with EVA. *Compos Struct*. 2003;62:391-395. https://doi.org/10.1016/j.compstruct.2003.09.010

39. Gregor-Svetec D, Leskovšek M, Vrabič Brodnjak U, Stankovič Elesini U, Muck D, Urbas R. Characteristics of HDPE/cardboard dust 3D printable composite filaments. *J Mater Process Technol*. 2020;276:39-47. https://doi.org/10.1016/j.jmatprotec.2019.116379

40. Menard KP, Menard NR. *Dynamic Mechanical Analysis*, 3rd ed., CRC Press, Boca Raton, FL, 2020. https://doi.org/10.1201/9780429190308

41. Nitta KH, Tanaka A. Dynamic mechanical properties of metallocene catalyzed linear polyethylenes. *Polymer (Guildf)*. 2001;42:1219-1226. https://doi.org/10.1016/S0032-3861(00)00418-3

42. Matsuo M, Bin Y, Xu C, Ma L, Nakaoki T, Suzuki T. Relaxation mechanism in several kinds of polyethylene estimated by dynamic mechanical measurements, positron annihilation, X-ray and 13C solid-state NMR, *Polymer (Guildf)*. 2003;44:4325-4340. https://doi.org/10.1016/S0032-3861(03)00352-5.

43. Munaro M, Akcelrud L. Correlations between composition and crystallinity of LDPE/HDPE blends. *J Polym Res*. 2008;15:83-88. https://doi.org/10.1007/s10965-007-9146-2

44. Popli R, Mandelkern L, Benson RS. Dynamic mechanical studies of alpha and beta relaxation of Polyethylenes. *J Polym Sci A-2*. 1984;22:407-448.

45. Mohagheghian I, McShane GJ, Stronge WJ. Impact perforation of monolithic polyethylene plates: projectile nose shape

dependence. *Int J Impact Eng.* 2015;80:162-176. https://doi.org/10.1016/j.ijimpeng.2015.02.002

46. Zhu S, Zhang Y, Zhang Y. Polyolefin composites filled with magnesium hydroxide. *Polym Polym Compos.* 2002;10:447-455. https://doi.org/10.1177/096739110201000605

47. Tadokoro H, Kobayashi M, Kawaguchi Y, Kobayashi A, Murahashi S. Normal vibrations of the polymer molecules of helical configuration. III. Polyoxymethylene and polyoxymethylene-d2. *J Chem Phys.* 1963;38:703-721. https://doi.org/10.1063/1.1733727

48. Ramirez NV, Sanchez-Soto M, Illescas S, Gordillo A. Thermal degradation of polyoxymethylene evaluated with FTIR and spectrophotometry. *Polym Plast Technol Eng.* 2009;48:470-477. https://doi.org/10.1080/03602550902725472

49. Keating MY, Sauer BB, Flexman EA. Dynamic mechanical characterization of relaxations in poly(oxymethylene), miscible blends, and oriented filaments. *J Macromol Sci Phys.* 1997;36:717-732. https://doi.org/10.1080/00222349708212398